Research Article

Preparation and Property of Mo-Doped Visible-Light Response Titaniumdioxide Photocatalyst

Yingying Li,[1] Xianliang Song,[1,2] Zhedong Wei,[1] Jianguang Zhang,[1] Lijuan Qin,[1] and Shengying Ye[1]

[1] *College of Food Science, South China Agricultural University, Guangzhou 510642, China*
[2] *Engineering Research Center of Starch and Plant Protein Processing, South China University of Technology, Ministry of Education, Guangzhou 510640, China*

Correspondence should be addressed to Xianliang Song; songxl2000@163.com

Mo-titaniumdioxide (P25) photocatalyst with visible-light response was prepared with the ammonium molybdate for Mo source and titaniumdioxide for the raw materials by the method of dissolving and calcining. The photocatalysts' structure was characterized by XRD, XPS, and UV-Vis absorption spectrum and TEM. The photocatalytic activities of Mo-titaniumdioxide were measured by the degradation of methylene blue (MB) under visible-light irradiation. The results showed that Mo characteristic peaks appeared at the point of 235.45 eV, 234.2 eV, 232.3 eV, and 231.1 eV. In Mo-titaniumdioxide crystal lattice, Mo^{6+} had the highest percentage (about 84.08%), indicating that Mo element was inserted into titaniumdioxide crystal lattice and considerable amount of Mo dopant was in the 6+ valence state, which restrained the recombination of electron-hole and had the visible-light photocatalytic activity. Photocatalytic degradation study indicated that the samples prepared at calcination temperature of 500°C were used to degrade MB; after 3 h, the degradation reached up to 80.67%.

1. Introduction

In recent years, studies of photocatalytic pollutant degradation have attracted more and more researchers' attention. In many semiconductor photocatalysts, nano-TiO_2 is most commonly used due to its high chemical stability, nontoxicity, and low cost, as well as high activity and good resistance to photocorrosion. However, it has been reported that the visible-light photocatalytic activity of TiO_2 is not usually satisfied because of its broadband gap (3.2 eV) which only responds to UV light ($\lambda < 387$ nm), which significantly restricts the practical application of TiO_2 [1–5].

In order to broaden the photoresponse range of TiO_2 from ultraviolet region to visible region and improve the availability of solar energy, many methods have been used to improve the photocatalytic property of TiO_2 which include metal ion doping (Cr, Ir, Co, etc.) [6–8], nonmetals ion doping (Cl, N, F, etc.) [9, 10], semiconductor compound (ZrO_2–TiO_2, Fe_2O_3–TiO_2, SnO_2–TiO_2, etc.) [11–13], and deposition of noble metal on the surface (Pd, Au, Ag, etc.) [14–16]. These modification methods mainly must be implemented through sol-gel method [17] and vapor deposition method [18] and so forth. Nevertheless, the visible-light responsive TiO_2 obtained with the addition of modified reagents often has certain characteristics such as larger particle size and smaller surface area. All these could result in the lower photocatalytic activity. In addition, the above synthetic methods often require harsh test conditions or special equipment, so industrial production is difficult to achieve.

P25 produced by German Degussa Company consists of 80% anatase phase and 20% rutile phase and its diameter ranges from 20 to 40 nm, which has the large specific surface area and is easy to obtain. Although P25 has a higher photocatalytic activity under UV-irradiation, its photocatalytic activity is low under sunlight or visible-light irradiation. Therefore, we directly modify P25 in order to obtain a high visible-light responsive photocatalyst; this research is a rewarding work. At the same time, few studies have been

reported to modify P25 so as to improve its photocatalytic activity. The study successfully prepared Mo-P25 photocatalyst with visible-light response and explored its visible-light photocatalytic activity.

2. Experiment

All chemicals were of analytical grade without further purification in this study. The Mo-P25 photocatalyst (hereinafter referred to as Mo-P25) was prepared with the method of dissolving and calcining. A certain amount of ammonium molybdate $((NH_4)_6Mo_7O_{24} \cdot 4H_2O)$ and P25 powders for which the molar percentage ratio of Mo element to Ti element was 0.85% were added to distilled water and stirred for 4 h. Thus, the mixed solution was transferred to the oven at 85°C and dried for 24 h. The dried sample was pulverized in the agate mortar for 0.5 h. The compounds were annealed in air ambient temperature at 300°C, 400°C, 500°C, 600°C, and 700°C for 3 h, respectively. The heating rate of all samples was 3°C/min.

The crystalline phases of the samples were determined by X-ray powder diffraction (XRD). The XRD spectra were taken at a Rigaku (Japan) D/max-IIIA X-ray diffractometer at 45 kV and 40 mA with Cu-Kα radiation (λ = 1.5406 nm), employing a scanning rate of $0.02° s^{-1}$ in the 2θ range from 15° to 85°. X-ray photoelectron spectroscopy (XPS) study was carried out using an ESCALAB 250 photoelectron spectrometer (Thermo Fisher Scientific) at 2.0×10^{-9} mbar with monochromatic Al Kα radiation (E = 1486.6 eV). UV-vis absorption spectra were recorded on a Hitachi U-3900 spectrophotometer. Transmission electron microscopy (TEM) image was collected by using a FEI Tecnai G212 microscope.

Methylene blue (MB) was used as a convenient photostable organic molecule to assay photocatalytic activities of Mo-P25. The prepared Mo-P25 (100 mg) was dispersed into an aqueous solution (200 mL) of methylene blue ($10 mgL^{-1}$). The suspension was sonicated for 15 min followed by stirring in dark for 30 min to ensure an adsorption-desorption equilibrium prior to irradiation. Then, the suspension was irradiated with a 85 W incandescent lamp while stirring. The solution of 10 mL was collected from the suspension after different reaction time and was immediately centrifuged at 6000 rpm for 15 min. The concentration of MB after illumination was determined spectrophotometrically at 664 nm by a UV-vis spectrophotometer. The photocatalytic activities of the catalysts were measured in terms of the degradation efficiency (%) of MB by the following equation:

$$\text{Degradation efficiency (\%)} = \frac{C_0 - C}{C_0} * 100, \qquad (1)$$

where C_0 is the initial concentration of MB and C is the concentration of MB after visible-light irradiation.

3. Results and Discussion

3.1. XRD Analysis. The XRD diffraction spectra of P25 and Mo-P25 with different calcination temperatures are shown
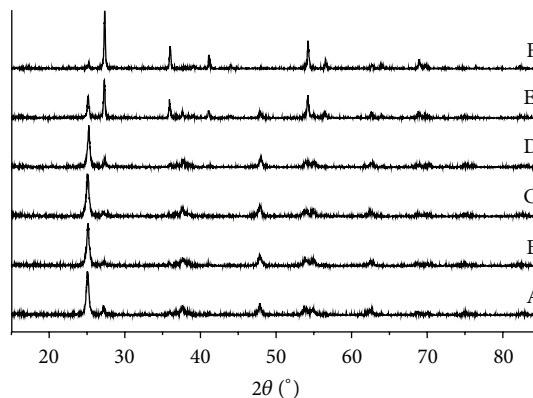

FIGURE 1: XRD spectra for samples with different calcination temperatures. A: P25, B, C, D, E, and F were Mo-P25 prepared at calcination temperature of 300°C, 400°C, 500°C, 600°C, and 700°C, respectively.

in Figure 1. As shown in Figure 1A, P25 which consists of 80% anatase phase and 20% rutile phase exhibited a good crystalline structure. The dominant peak at 25.3° was indexed as (101) plane of anatase phase. Compared with A, the dope of Mo made the diffraction angle of the (101) peak of P25 shift from a certain angle to a higher angle, which indicated that the addition of Mo could induce crystal lattice defects of P25. Figure 1B and Figure 1C suggested that when calcination temperatures were 300°C and 400°C, the diffraction peaks of rutile phase became weaker than P25, which showed that Mo could restrain the growth of rutile phase, obviously (110) plane of rutile phase. With calcination temperature increasing to 500°C, a few of anatase phases were transformed to rutile phase initially, but not apparently. When calcination temperature reached 600°C, the diffraction peaks of rutile phase became sharp, indicating that anatase phase was transformed to rutile phase gradually. By further increase of calcination temperature to 700°C, anatase phase disappeared nearly. No obvious peaks of Mo could be detected; this was because the ionic radius of Mo^{6+} was 0.062 nm and that of Ti^{4+} was 0.068 nm; Mo^{6+} was incorporated into P25 crystal lattice. And the doping quantity may be so small that the XRD instruments could not detect its signal.

3.2. XPS Analysis. Figure 2 shows that a peak appearing at the range from 200 eV to 300 eV was Mo element characteristic peak, which fairly accorded with experimental result reported in [19], indicating that Mo element was incorporated into P25 crystal lattice successfully. The three bands which appeared at 531 eV, 458.7 eV, and 284 eV were ascribed to the O(1s), Ti(2p), and C(1s), respectively, and C(1s) characteristic peak was caused by carbon contamination in the test system. Table 1 shows that the atomic percentage of Mo was only 0.8% in Mo-P25 samples by XPS which was corresponding with the detection results of XRD. The doping amount of Mo element was so little that it could not change the main crystal structure of P25.

Figure 3 shows that the deconvolution of Mo(3d) peak resulted in four peaks centered at 235.45 eV, 234.2 eV, 232.3 eV,
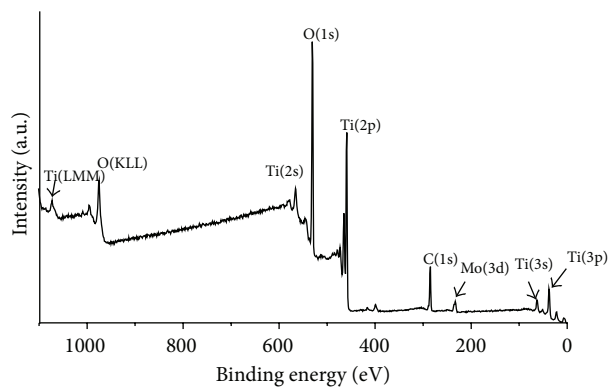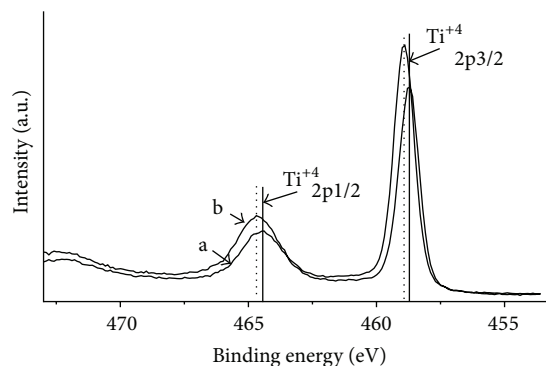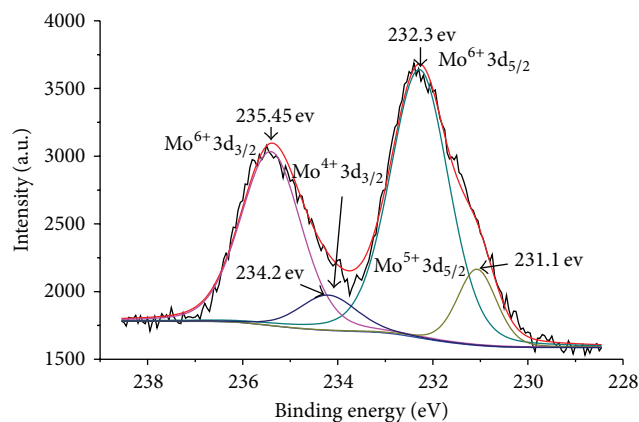
FIGURE 2: XPS spectra of Mo-P25.

FIGURE 3: XPS spectra of Mo element.

TABLE 1: The atomic content of Mo-P25.

Peak	Position BE (eV)	Raw area (CPS)	Atomic conc. %
C(1s)	284.81	17833.21	25.14
O(1s)	530.16	88892.73	53.54
Ti(2p)	458.92	96617.39	20.52
Mo(3d)	232.39	6363.95	0.8

TABLE 2: The content of different Mo valence state.

Mo species analysis				
Name	Energy (ev)	FWHM	Area	Ti/at%
$Mo^{6+}\ 3d_{3/2}$	235.41	1.5	2250.084	33.73184
$Mo^{6+}\ 3d_{5/2}$	232.28	1.45	3358.334	50.34603
$Mo^{5+}\ 3d_{5/2}$	231.07	0.97	635.9796	9.534206
$Mo^{5+}\ 3d_{3/2}$	234.2	1.4	426.1064	6.387919

and 231.1 eV. According to the PEAKFIT resolved peaks and literatures [20], the peaks were identified as Mo^{6+} and Mo^{5+}. Every valent Mo content was obtained by dealing with detection results which is listed in Table 2. As shown in Table 2, Mo^{6+} had the highest percentage (more than 80%), indicating that Mo element was incorporated into P25 crystal lattice and considerable amount of Mo was in the 6+ valence state.

FIGURE 4: XPS spectra of Ti element of P25 and Mo-P25, respectively. a: Ti element of P25. b: Ti element of Mo-P25.
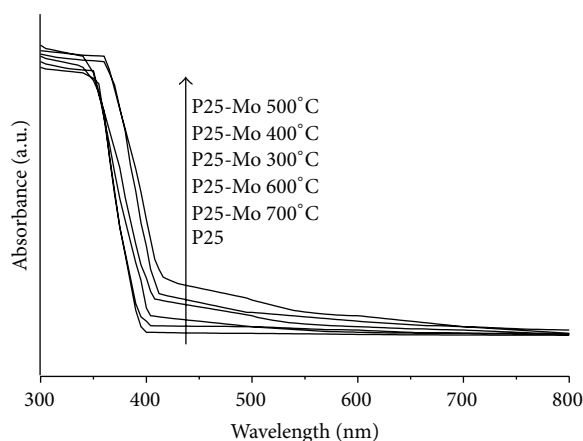

FIGURE 5: UV-vis spectra for P25 and Mo-P25 calcined at different temperatures.

XPS spectra of Ti element of P25 and Mo-P25 were shown in Figure 4. As shown in Figure 4a, the binding energy of Ti2p1/2 was 464.5 eV which was higher than that (458.7 eV) for Ti2p3/2; peak patterns of Ti2p1/2 and Ti2p3/2 presented a symmetric distribution, so the peaks of Ti were identified as Ti^{4+} characteristic peak. As shown in Figure 4b, compared with Figure 4a, the binding energy of Ti peak was shifted to higher binding energy; this was because Mo doped into P25 crystal lattice had higher chemical valence state than Ti of P25 and seized the oxygen atom of P25 crystal lattice to form Mo_xO_y, which led to the decrease of Ti electron density and the increase of Ti binding energy.

3.3. UV-Vis Analysis. Figure 5 shows that P25 almost did not have photoabsorption in the visible region. However, Mo-P25 prepared at different calcination temperatures had strong photoabsorption accompanied with red shift phenomenon; this was due to the dope of Mo which caused lattice defects of P25, along with the distortion of crystal lattice. All these contributed to producing more oxidation centers in Ti^{3+} and greatly decreased the recombination of electron and hole which made light response region shift to visible-light region and improved the visible-light photocatalytic

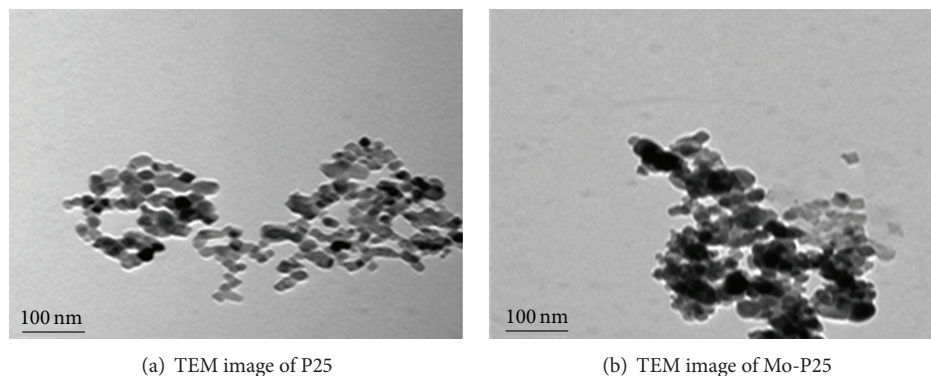(a) TEM image of P25

(b) TEM image of Mo-P25

FIGURE 6: TEM images of P25 and Mo-P25.

activity. However, different calcination temperature had an obvious influence on the visible photoabsorption of Mo-P25. When calcination temperature was 500°C, a few of anatase phases were transformed to rutile phase initially and mixed crystal effect was generated under the giant amount of anatase phase and the small amount of rutile phase which had evident positive effect on the improvement of visible photoabsorption. When calcination temperature reached 700°C, the photoabsorption of Mo-p25 decreased rapidly in visible-light region. This was because that anatase phase almost disappeared, and rutile phase was transformed from anatase phase which was mostly inactive. When calcination temperature was 300°C, the visible photoabsorption and red shift phenomenon of Mo-P25 were not evident; this was because calcination temperature was too low and Mo element was hardly incorporated into P25 crystal lattice.

3.4. TEM Analysis. Figure 6(a) shows that P25 particles were uniform in size with the range dimension of 20–40 nm by means of ultrasonic dispersion. Compared with Figure 6(a), Figure 6(b) shows that Mo-P25 nanoparticles were agglomerated easily in aqueous solution and were irregular in shape; the reason was that Mo^{6+} substituted Ti^{4+} in P25 crystal lattice and this substitution caused lattice defects.

3.5. Photocatalytic Activity Test. Figure 7 shows that the photocatalytic activities of Mo-P25 and P25 with different calcination temperatures were evaluated under visible-light irradiation. As shown in Figure 7, the visible photocatalytic activity of P25 was very low whose degradation efficiency of MB was 1.58%. When calcination temperature was 500°C, Mo-P25 presented the best photocatalytic activity, and the degradation efficiency of MB reached 80.67%. With calcination temperature continuing to increase, the photocatalytic activity of Mo-P25 dropped obviously. When calcination temperature was up to 700°C, the degradation efficiency of MB was lowest, which was only 1.36%. All these indicated that calcination temperature had a significant effect on the photocatalytic activity of Mo-P25. When calcination temperature was lower, heat energy hardly made P25 crystal phase transform and never let Mo be incorporated into P25 crystal lattice. However, when calcination temperature was higher,
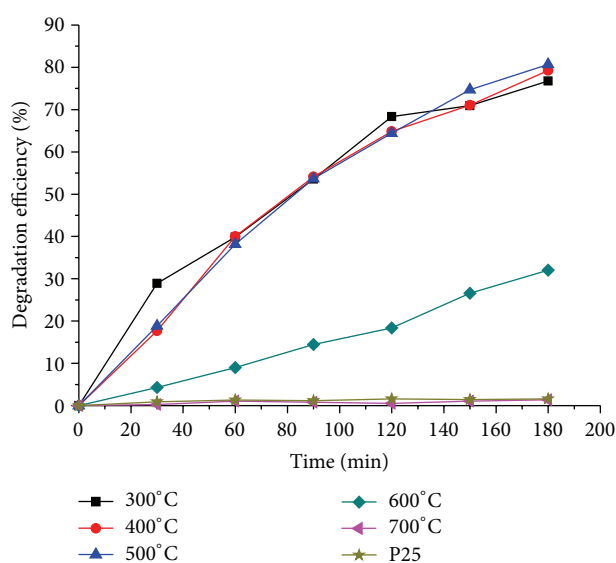

FIGURE 7: Photocatalytic activity of Mo-P25 and P25 with different calcination temperatures.

enough heat energy made almost all anatase phase transform to rutile phase, which would reduce the photocatalytic activity. Therefore, with calcination temperature increasing, the photocatalytic activity of Mo-P25 presented the downward trend after the first rise.

4. Conclusion

Mo-P25 photocatalysts were prepared by the method of dissolving and calcining. The photocatalytic activities of Mo-P25 samples prepared at different calcination temperature were measured by measuring the degradation of methylene blue. The results showed that calcination temperature was an important factor affecting the photocatalytic activity. When calcination temperature was 500°C, Mo-P25 photocatalyst presented the best photocatalytic activity and the degradation efficiency of MB reached up to 80.67%. The structure characterization of Mo-P25 prepared at different calcination temperature indicated that when calcination temperature was

500°C, a few of anatase phases were transformed to rutile phase initially. With calcination temperature increasing to 700°C, almost all anatase phase was transformed to rutile phase. By calcining Ti^{4+} was substituted for Mo^{6+} into P25 crystal lattice. The visible photoabsorption was improved under the action of Mo dopant. The red shift of the absorption spectrum took place evidently. All these were contributed to the increase of the photocatalytic activities of Mo-P25.
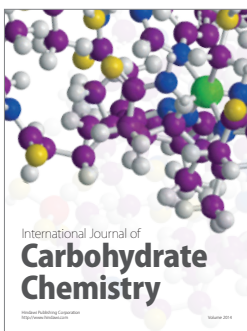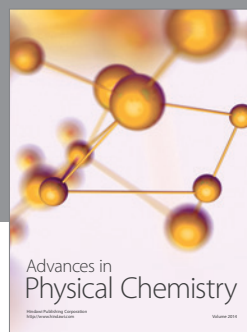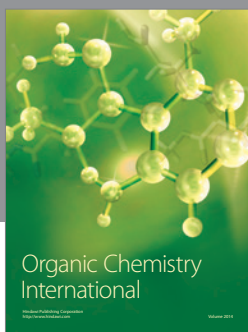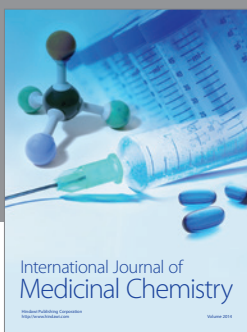
Conflict of Interests

The authors declare that there is no conflict of interests regarding the publication of this paper.

Acknowledgments

References

[1] S. H. Lim, C. Ferraris, M. Schreyer, K. Shih, J. O. Leckie, and T. J. White, "The influence of cobalt doping on photocatalytic nano-titania: crystal chemistry and amorphicity," *Journal of Solid State Chemistry*, vol. 180, no. 10, pp. 2905–2915, 2007.

[2] K. Nagaveni, G. Sivalingam, M. S. Hegde, and G. Madras, "Solar photocatalytic degradation of dyes: high activity of combustion synthesized nano TiO_2," *Applied Catalysis B: Environmental*, vol. 48, no. 2, pp. 83–93, 2004.

[3] O. Carp, C. L. Huisman, and A. Reller, "Photoinduced reactivity of titanium dioxide," *Progress in Solid State Chemistry*, vol. 32, no. 1-2, pp. 33–177, 2004.

[4] M. Hamadanian, A. Reisi-Vanani, and A. Majedi, "Synthesis, characterization and effect of calcination temperature on phase transformation and photocatalytic activity of Cu,S-codoped TiO_2 nanoparticles," *Applied Surface Science*, vol. 256, no. 6, pp. 1837–1844, 2010.

[5] X. Cheng, X. Yu, and Z. Xing, "One-step synthesis of visible active CNS-tridoped TiO_2 photocatalyst from biomolecule cystine," *Applied Surface Science*, vol. 258, no. 19, pp. 7644–7650, 2012.

[6] S. J. Zhang, "Synergistic effects of C-Cr codoping in TiO_2 and enhanced sonocatalytic activity under ultrasonic irradiation," *Ultrasonics Sonochemistry*, vol. 19, no. 4, pp. 767–771, 2012.

[7] P. Chen, J. Lu, G. Xie, L. Zhu, and M. Luo, "Characterizations of Ir/TiO_2 catalysts with different Ir contents for selective hydrogenation of crotonaldehyde," *Reaction Kinetics, Mechanisms and Catalysis*, vol. 106, no. 2, pp. 419–434, 2012.

[8] S.-Y. Liu, W.-H. Tang, Q.-G. Feng, J.-Z. Li, and J.-H. Sun, "Synthesis of N, Fe Co-doped TiO_2 nanomaterials via solid state reaction and their photodegradation of quinoline irradiated under visible light," *Journal of Inorganic Materials*, vol. 25, no. 9, pp. 921–927, 2010.

[9] X.-K. Wang, C. Wang, W.-Q. Jiang, W.-L. Guo, and J.-G. Wang, "Sonochemical synthesis and characterization of Cl-doped TiO_2 and its application in the photodegradation of phthalate ester under visible light irradiation," *Chemical Engineering Journal*, vol. 189-190, pp. 288–294, 2012.

[10] W. Wang, C. H. Lu, Y. R. Ni, M. X. Su, W. J. Huang, and Z. Z. Xu, "Preparation and characterization of visible-light-driven N-F-Ta tri-doped TiO_2 photocatalysts," *Applied Surface Science*, vol. 258, no. 22, pp. 8696–8703, 2012.

[11] A. Naumenko, I. Gnatiuk, N. Smirnova, and A. Eremenko, "Characterization of sol-gel derived TiO_2/ZrO_2 films and powders by Raman spectroscopy," *Thin Solid Films*, vol. 520, no. 14, pp. 4541–4546, 2012.

[12] Q. Sun, W. Leng, Z. Li, and Y. Xu, "Effect of surface Fe_2O_3 clusters on the photocatalytic activity of TiO_2 for phenol degradation in water," *Journal of Hazardous Materials*, vol. 229-230, pp. 224–232, 2012.

[13] B. C. Yadav, N. Verma, and S. Singh, "Nanocrystalline SnO_2-TiO_2 thin film deposited on base of equilateral prism as an optoelectronic humidity sensor," *Optics and Laser Technology*, vol. 44, no. 6, pp. 1681–1688, 2012.

[14] A. Yildiz, D. Crisan, N. Dragan, N. Iftimie, D. Florea, and D. Mardare, "Effect of formaldehyde gas adsorption on the electrical conductivity of Pd-doped TiO_2 thin films," *Journal of Materials Science: Materials in Electronics*, vol. 22, no. 9, pp. 1420–1425, 2011.

[15] T. Nogawa, T. Isobe, S. Matsushita, and A. Nakajima, "Preparation and visible-light photocatalytic activity of Au- and Cu-modified TiO_2 powders," *Materials Letters*, vol. 82, pp. 174–177, 2012.

[16] V. Mirkhani, S. Tangestaninejad, M. Moghadam, M. H. Habibi, and A. Rostami Vartooni, "Photodegradation of aromatic amines by Ag-Tio_2 photocatalyst," *Journal of the Iranian Chemical Society*, vol. 6, no. 4, pp. 800–807, 2009.

[17] X. Zhang, H. Yang, F. Zhang, and K.-Y. Chan, "Preparation and characterization of Pt-TiO_2-SiO_2 mesoporous materials and visible-light photocatalytic performance," *Materials Letters*, vol. 61, no. 11-12, pp. 2231–2234, 2007.

[18] X.-X. Wang, X. Chen, H.-B. Xu, and X.-Z. Fu, "Advance in modification method of zeolite molecular sieve surface," *Chinese Journal of Inorganic Chemistry*, vol. 18, no. 6, pp. 541–549, 2002.

[19] Y. Shen, T. Xiong, H. Du, H. Jin, J. Shang, and K. Yang, "Phosphorous, nitrogen, and molybdenum ternary co-doped TiO_2: preparation and photocatalytic activities under visible light," *Journal of Sol-Gel Science and Technology*, vol. 50, no. 1, pp. 98–102, 2009.

[20] O. Y. Khyzhun, T. Strunskus, and Y. M. Solonin, "XES, XPS and NEXAFS studies of the electronic structure of cubic $MoO_{1.9}$ and $H_{1.63}MoO_3$ thick films," *Journal of Alloys and Compounds*, vol. 366, no. 1-2, pp. 54–60, 2004.